JACS
JOURNAL OF THE AMERICAN CHEMICAL SOCIETY
pubs.acs.org/JACS
Article

Superconductivity at 31 K in a Stage-1 Sodium-Intercalated Graphite

Yuan-Qing Liu,[#] Ming-Xing Huang,[#] Chun-Mei Hao,[#] Jingyu Hou, Guochun Yang, Jiajia Feng, Bin Chen, Yang Ding, Shaobo Yu, Jian Sun, Lin Wang, Bo Xu, Feng Ke,* Xiang-Feng Zhou,* and Yongjun Tian*

Cite This: *J. Am. Chem. Soc.* 2026, 148, 34888−34894

Read Online

ACCESS | Metrics & More | Article Recommendations | Supporting Information

ABSTRACT: Graphite intercalation compounds (GICs) serve as a highly tunable platform for exploring phonon-mediated superconductivity in lightweight materials. While theoretical models have long predicted that densely packed, first-stage (stage-1) sodium-intercalated graphite (Na-GIC) could host elevated critical temperatures (T_c), its experimental synthesis has remained a formidable challenge. Here, we report the realization of stage-1 Na-GIC that exhibits bulk superconductivity and achieves a maximum onset T_c of ∼31 K, setting a record for all known GIC systems. By employing a room-temperature mechanical synthesis with an excess sodium reservoir, followed by lattice compression, we force a sequential staging transition in Na-GIC—from an initial stage-8, through an intermediate stage-2, and ultimately to the densely intercalated stage-1 phase at 15.6 GPa. By correlating room-temperature in situ synchrotron X-ray diffraction with evolutionary structural searches, we identify the host of this high-T_c state as an orthorhombic NaC_3 structure with *Imma* symmetry. First-principles calculations reveal a remarkably strong electron−phonon coupling ($\lambda \sim 2.0$), dominated by interactions between out-of-plane carbon π electrons and low-frequency Na/C vibrations. Our findings not only capture the elusive stage-1 Na-GIC but also establish pressure-driven compositional tuning as a robust strategy to unlock high-T_c states in carbon-based superlattices.

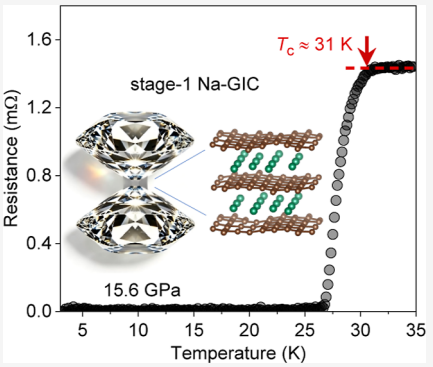

INTRODUCTION

Within the conventional Bardeen−Cooper−Schrieffer (BCS) framework,[1] achieving a high superconducting transition temperature (T_c) relies on high phonon frequencies and strong electron−phonon coupling (EPC), pointing naturally to materials composed of light elements such as hydrogen, lithium, boron, carbon, sodium, and magnesium. The discovery of near-room-temperature superconductivity in hydrogen-rich compounds provides a compelling demonstration that electron−phonon-mediated superconductivity can achieve T_c exceeding the boiling temperature of liquid nitrogen and even approaching room temperature, albeit only under ultrahigh pressures.[2−4] At ambient pressure, magnesium diboride (MgB_2, T_c = 39 K) remains the benchmark,[5] where a stiff, lightweight boron network provides the high-frequency phonons necessary to enable strong coupling between electronic states and lattice vibrations. Replicating this MgB_2-like structural motif in other systems to surpass the McMillan limit (∼40 K) has been a central, yet largely unrealized goal in materials science and condensed matter physics.[6−11]

Graphite intercalation compounds (GICs) offer a highly tunable, structurally analogous platform to MgB_2. By inserting guest atoms between graphene layers, charge transfer populates the carbon π^* bands and introduces new interlayer electronic states, fostering emergent quantum phenomena such as superconductivity.[12−18] Superconductivity in GICs was first reported in KC_8, with a T_c of approximately 0.55 K.[19] Subsequent advances were realized in CaC_6, which exhibits a T_c of 11.5 K at ambient pressure[20,21] and 15.1 K at 7.5 GPa.[22,23] Building on this trajectory, recent high-pressure breakthroughs have dramatically advanced the field, demonstrating T_c values of 22−28 K in stage-2 sodium-intercalated graphite (Na-GICs).[24,25] These discoveries have reinvigorated the community, particularly because ab initio calculations predicted that a densely packed, first-stage (stage-1) Na-GIC could sustain even higher T_c values—up to 41 K at 5 GPa and 48 K at 10 GPa—[26,27]driven by optimal coupling between carbon π electrons and Na/C vibrations. Yet, the experimental realization of stage-1 Na-GIC has remained fundamentally elusive due to the formidable thermodynamic barriers associated with fully intercalating every graphene interlayer.

Received: May 27, 2026
Revised: July 22, 2026
Accepted: July 24, 2026
Published: August 1, 2026

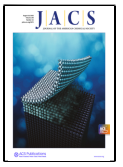

https://doi.org/10.1021/jacs.6c10866
J. Am. Chem. Soc. 2026, 148, 34888−34894

RESULTS AND DISCUSSION

Our prior work demonstrated that room-temperature grinding of sodium and graphite (with a molar ratio of Na/C = 1:6) yields a stage-8 Na-GIC with a fraction of unreacted sodium.[24] Under compression, this residual sodium acted as an intercalant reservoir, progressively entering the graphite host to form a superconducting stage-2 NaC_8 with a maximum T_c of 22.3 K at ~7 GPa (denoted SC1, Figure 1a). This pressure-driven intercalation mechanism suggests that increasing the initial sodium content may force the system into even more densely intercalated states. Accordingly, we adopted a highly Na-rich precursor (Na/C = 1:3). While ambient-pressure XRD confirms the product remains a stage-8 GIC (Figure S1),[24,28] it contains a substantially larger Na intercalation reservoir. Here, by compressing this Na-rich precursor, we overcome the synthetic barrier and report the realization of a stage-1 Na-GIC that exhibits bulk superconductivity and achieves a maximum onset T_c of ~31 K. We discovered a new dome-shaped superconducting phase (denoted SC2, Figure 1a) whose record-breaking T_c and bulk nature are unambiguously confirmed by zero electrical resistance and pronounced diamagnetism, respectively. Correlating room-temperature in situ synchrotron XRD with first-principles calculations reveals the underlying structural evolution: a sequential staging transition from the initial stage-8 phase, through an intermediate stage-2, and ultimately to the densely intercalated stage-1 Na-GIC that hosts the observed high-T_c superconductivity (Figure 1b).

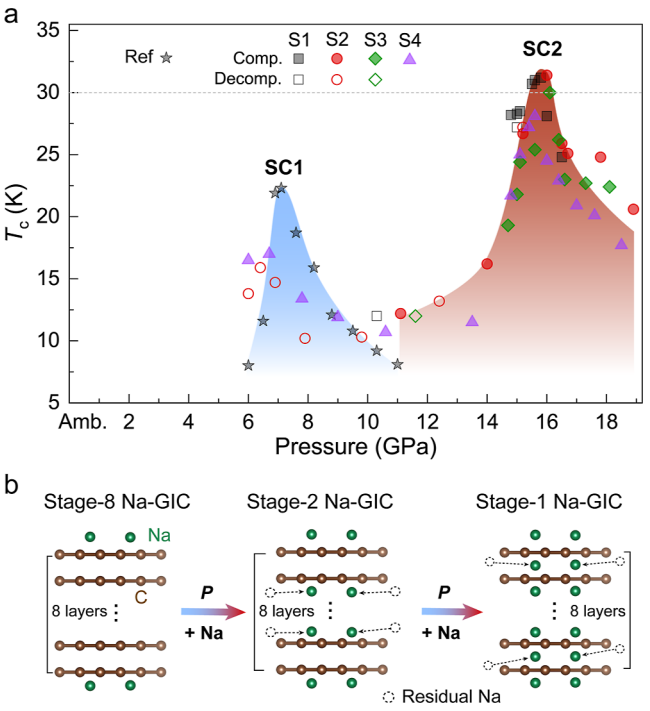

Figure 1. Superconductivity and schematic structural evolution of Na-GIC under compression. (a) Superconducting transition temperature (T_c) vs pressure. Star symbols denote the experimentally reported T_c values for the stage-2 NaC_8 phase.[24] The two distinct superconducting domes, labeled SC1 and SC2, correspond to independent measurements on separate Na-GIC samples synthesized via mechanical grinding with initial Na/C molar ratios of 1:6 and 1:3, respectively. (b) Schematic of the pressure-driven sodium intercalation into graphite. Applied pressure forces residual sodium into the graphite host, driving a sequential structural transition from the initial ambient-pressure stage-8 phase, through an intermediate stage-2 phase, and ultimately to the densely intercalated stage-1 phase.

To establish the superconducting properties of the densely intercalated SC2 Na-GIC, we performed low-temperature electrical transport measurements under compression. The inset of Figure 2a presents the temperature-dependent electrical resistance of Na-GIC at 15.6 GPa, the optimal pressure for the highest T_c. Upon cooling, the resistance exhibits metallic behavior ($dR/dT > 0$), which is followed by an abrupt drop initiating at an onset T_c of ~31 K and ultimately reaching a zero-resistance state at ~26.7 K—the defining hallmark of a superconducting transition. This superconducting transition is exceptionally sensitive to the applied pressure (Figure 2a); the maximum $T_c \approx 31$ K is sustained only within a narrow pressure window of ~1 GPa centered at 15.6 GPa. Tuning the pressure either below or above this optimal value substantially suppresses T_c, yielding the characteristic superconducting dome of the SC2 phase (Figure 1a). This dome-like behavior is highly reproducible across multiple independent measurements (samples S2–S4, Figure S2), with only minor variations in the optimal pressure and peak T_c values, verifying the intrinsic robustness of the superconducting transition. Furthermore, the transition remains nearly reversible during compression–decompression cycles, underscoring the resilience of the pressure-induced superconducting phase in the SC2 Na-GIC. Notably, the peak T_c of ~31 K in this SC2 phase surpasses the boiling point of liquid neon (~27.1 K), setting a new record among all experimentally achieved GICs.

The superconducting nature of the SC2 Na-GIC is further corroborated by its responses to external magnetic fields and by magnetic susceptibility measurements. As shown in Figure 2b, applying a magnetic field progressively shifts the superconducting transition to lower temperatures while the normal-state resistance remains invariant, an observation that distinctly separates superconductivity from conventional magnetoresistance effects. Fitting the temperature dependence of the upper critical field (Figure 2c) using the Ginzburg–Landau (GL) model[29] yields a zero-temperature upper critical magnetic field, $H_{c2}(0)$, of 9.2 ± 0.2 T and a corresponding GL coherence length of 5.98 ± 0.06 nm. This $H_{c2}(0)$ value is significantly higher than that of CaC_6[21] but remains lower than that of bulk MgB_2,[30] suggesting an intermediate electron–phonon coupling. Crucially, zero-field-cooled (ZFC) magnetization measurements reveal pronounced diamagnetic responses at ~15 K and ~24 K under representative pressures of 16.6 and 19.1 GPa, respectively (Figures 2d and S3). Derived from the ZFC data, the superconducting volume fraction of ~89.3% at 19.1 GPa (Figure S3) provides compelling evidence for bulk superconductivity in the SC2 phase. While the absolute maximum T_c of ~ 31 K is not perfectly captured in the magnetization data set—a consequence of the extremely narrow optimal pressure window for this high-T_c state and inherent difference in detection sensitivity between resistance and magnetization probes—the magnetization T_c (e.g., ~24 K at 19.1 GPa) aligns remarkably well with the zero-resistance temperature [T_c (R = 0) = 23–27 K] measured across four independent transport samples, as diamagnetism emerges with the establishment of a zero-resistance superconducting state. The slight pressure offsets between the electrical transport and magnetization data sets are characteristic of pressure gradients (Figure S4) commonly encountered in diamond anvil cell

https://doi.org/10.1021/jacs.6c10866
J. Am. Chem. Soc. 2026, 148, 34888–34894

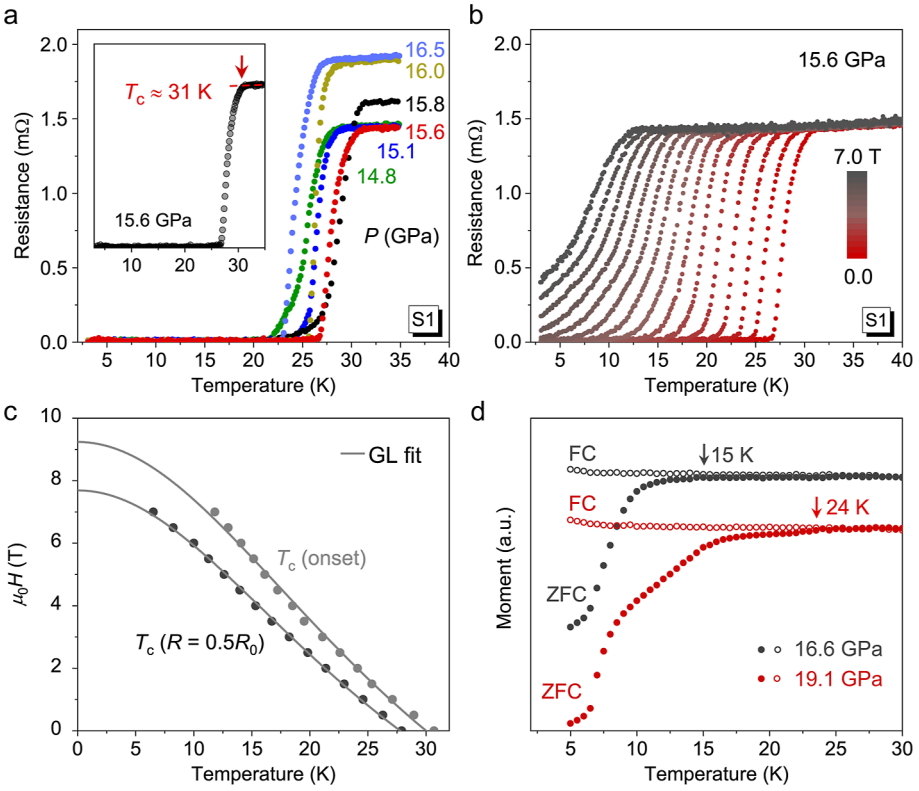

Figure 2. Electrical transport and magnetization evidence for superconductivity in the SC2 Na-GIC. (a) Temperature-dependent resistance curves obtained during compression, showing the pressure-tuned superconductivity. (b) Suppression of T_c under external magnetic fields at 15.6 GPa. (c) Ginzburg–Landau (GL) fitting of the H (T) versus T_c curves. T_c is defined by both the onset of the superconducting transition [T_c (onset)] and the half-normal-state resistances [T_c ($R = 0.5R_0$)]. (d) Zero-field-cooled (ZFC) and field-cooled (FC) magnetization data at 16.6 and 19.1 GPa, obtained after subtracting the background signals of the DAC and the nonmagnetic rhenium gasket.

(DAC) experiments, a phenomenon well documented in other high-pressure superconductors.[31−34] Furthermore, the different pressure calibration methods (ruby for electrical transport and diamond Raman edge for magnetization measurements) may also play a non-negligible role in the pressure offsets.[35,36]

To elucidate the crystal structure of the pressure-induced superconducting SC2 phase, we performed synchrotron XRD on powdered samples using a rigorous two-step experimental protocol. First, we conducted low-temperature electrical resistance measurements to identify the optimal pressure yielding the maximum $T_c \approx 31$ K. Subsequently, we performed in situ XRD measurements at this precalibrated pressure to determine the corresponding crystallographic structure and its evolution with pressure. Two independent experimental runs, initially at 16.8 GPa (Figure 3a) and 15.8 GPa (Figure S5), yielded a highly consistent XRD data set. Upon further compression to 20.1 GPa and subsequent partial decompression to 9.5 GPa, the XRD patterns remain nearly identical aside from minor variations in relative peak intensities (Figure 3a), underscoring the structural robustness of the superconducting SC2 phase at these elevated pressures.

However, when the pressure is released further down to 5.1 GPa, two new characteristic peaks (marked by red triangles in Figure 3a) emerge at $2\theta \approx 4.19°$ ($d \approx 7.419$ Å) and 8.37° ($d \approx 3.717$ Å). The appearance of these diffraction peaks indicates the breakdown of SC2 and the formation of a stage-2 Na-GIC structure (SC1 phase), consistent with a previous study.[24] A structural model (Figure S6) comprising a majority stage-2 NaC_8 and a minority stage-2 NaC_6 phases achieves an exceptional Le Bail fit to the 5.1 GPa XRD pattern (Figure 3b). Notably, a broad diffraction feature attributable to element sodium reappears at this pressure (black triangle, Figure 3a), signaling the partial deintercalation of sodium from the graphite host during decompression. This observation implies that the sodium intercalation stoichiometry is highly pressure-dependent, with a lower intercalation stage (higher sodium content) stabilized at elevated pressures. Consistent with this, no diffraction peaks from elemental sodium were observed in the 16.8 GPa pattern (Figure S7). This strongly indicates that the SC2 phase, which hosts the 31 K superconductivity, is a densely intercalated, lower-stage Na-GIC relative to the stage-2 NaC_8 phase—specifically, a stage-1 Na-GIC.

We simulated XRD patterns for all thermodynamically stable Na–C compounds documented in prior studies;[26,27] however, none of these previously reported structures—including the recently reported *Cmcm*-NaC_8 phase[25]—matched our experimental data (Figure S7). To infer the crystal structure of the emergent SC2 phase, we performed variable-composition structural searches using the evolutionary algorithm USPEX to predict thermodynamically stable compounds in the Na–C system at 15 GPa (Figure 4a). Among the generated candidates, a stage-1 NaC_3 phase with *Imma* symmetry emerges very close to the convex hull, possessing a formation enthalpy of ∼−0.13 eV/atom. This indicates that while this phase is metastable under pressure, it is synthetically accessible. Strikingly, detailed structural analysis using the GSAS software reveals that this *Imma*-NaC_3 structure perfectly captures the dominant experimental diffraction features (Figure 3c and d). Le Bail refinement yields lattice parameters of $a = 4.441 \pm$

https://doi.org/10.1021/jacs.6c10866
J. Am. Chem. Soc. 2026, 148, 34888−34894

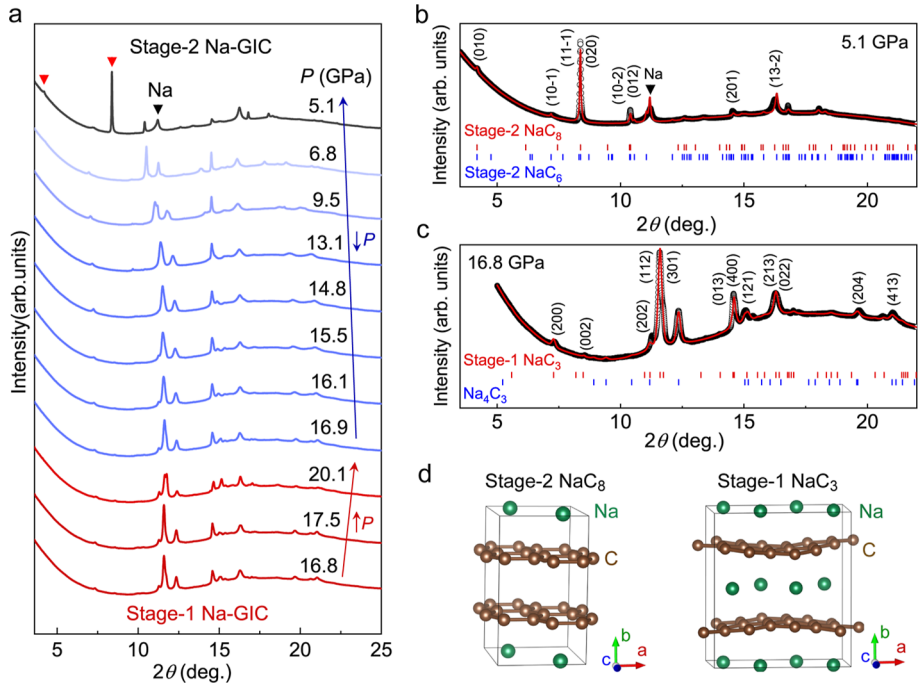

Figure 3. Crystal structure characterization of Na-GIC under compression and decompression. (a) Room-temperature synchrotron XRD patterns (X-ray wavelength of 0.5427 Å) at representative pressures. Triangles mark the characteristic peaks of the stage-2 Na-GIC (red) and deintercalated sodium (black) at 5.1 GPa. (b) Le Bail fitting of the XRD pattern at 5.1 GPa upon decompression (open circles: experimental data; red line: fitted profile) using structural models comprising stage-2 NaC_8 (*Pmma*), NaC_6 (*P*2/*m*), and elemental sodium. Vertical ticks indicate the indexed peaks of NaC_8 (red) and NaC_6 (blue). (c) Le Bail refinement of the XRD pattern at 16.8 GPa using structural models consisting of stage-1 NaC_3 (*Imma*) and Na_4C_3 ($R\bar{3}m$). Vertical ticks denote the indexed peaks of NaC_3 (red) and Na_4C_3 (blue). (d) Crystal structures of stage-2 NaC_8 and stage-1 NaC_3. Sodium and carbon atoms are colored in green and brown, respectively.

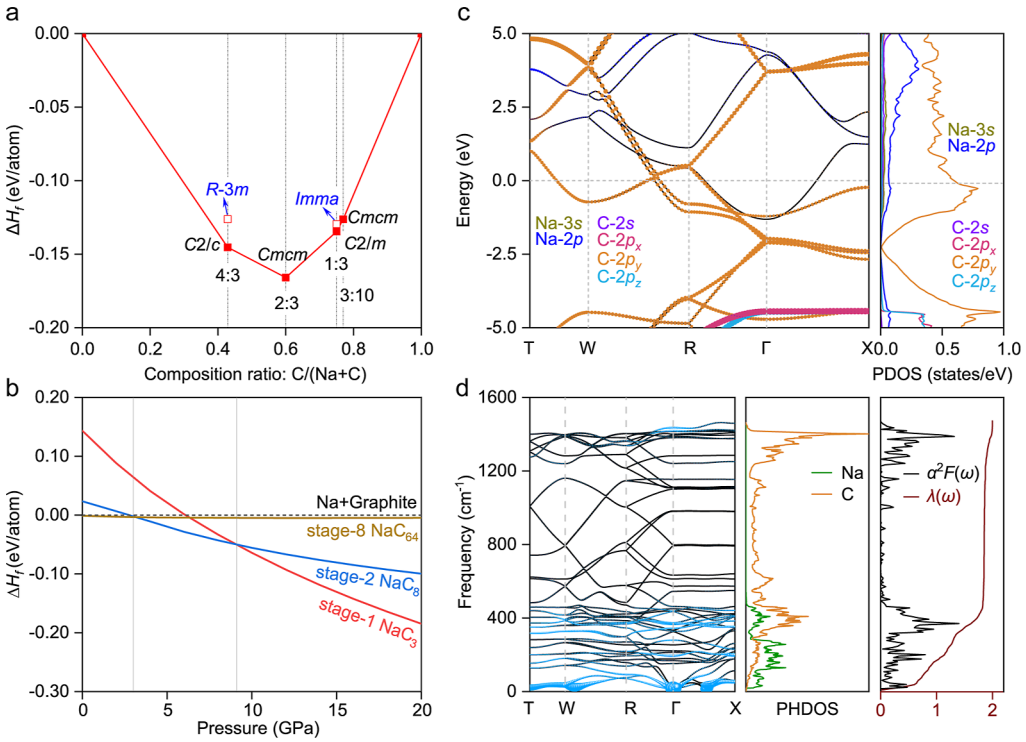

Figure 4. Composition-dependent formation energy, electronic structure, and EPC analysis of *Imma*-NaC_3 at 15 GPa. (a) Formation enthalpies for Na−C compounds at 15.0 GPa relative to elemental sodium and graphite. (b) Formation enthalpies for stage-8 NaC_{64} (yellow), stage-2 NaC_8 (blue), and stage-1 NaC_3 (red) at high pressures, referenced to sodium and graphite (black dashed line). (c) Orbital-resolved electronic band structure and projected density of states (PDOS). Note that the lattice vector *b* is oriented along the stacking direction. (d) Phonon dispersion curve, projected phonon DOS (PHDOS), Eliashberg spectral function $\alpha^2F(\omega)$, and the accumulated EPC strength $\lambda(\omega)$.

https://doi.org/10.1021/jacs.6c10866
J. Am. Chem. Soc. 2026, 148, 34888−34894

0.021 Å, b = 8.539 ± 0.025 Å, and c = 7.336 ± 0.023 Å at 16.8 GPa, in excellent agreement with the theoretically calculated lattice constants (a = 4.334 Å, b = 8.528 Å, and c = 7.461 Å at 15 GPa). We note that several diffraction peaks ($2\theta \approx 12.3°$, 15.0°, and 19.6°) remained unindexed in this NaC_3 structure. These unassigned peaks were found to match a Na_4C_3 structure adopting $R\bar{3}m$ symmetry (Figure S8). Incorporating both phases in our refinement model yields an exceptional fit to the experimental data (Figure 3c), suggesting the coexistence of a majority *Imma*-NaC_3 phase and a minority $R\bar{3}m$-Na_4C_3 phase within the sample. Collectively, our in situ XRD and theoretical results demonstrate pressure-driven sequential staging transitions in Na-GIC: from the initial ambient-pressure stage-8 phase, through an intermediate stage-2 phase, and ultimately to the densely intercalated, superconducting SC2 phase—which we identify here as a stage-1 Na-GIC adopting an orthorhombic *Imma* structure. First-principles calculations (Figure 4b) further corroborate the structural evolution and energetic stability of Na-GICs under pressure: stage-8 NaC_{64} has lower energy than competing phases and is thermodynamically favored below ~3 GPa, followed by stabilization of stage-2 NaC_8 with increasing pressure and stage-1 NaC_3 above ~9 GPa. Molecular dynamics simulations (Figures S9 and S10) provide further insight into the dynamic formation of the stage-1 phase. Above 9 GPa, sodium atoms spontaneously intercalate into graphite interlayers, with the Na/C ratio converging to approximately 1:3. These results are quantitatively consistent with the NaC_3 stoichiometry identified through both experiments and DFT-based global structure searches.

To investigate the pairing mechanism driving this high-temperature superconductivity, we performed systematic EPC calculations on the proposed *Imma*-NaC_3 structure of the SC2 phase (Figure 4c,d). The calculations yield a large EPC parameter of λ = 2.0 and a logarithmic average phonon frequency of ω_{log} = 197.1 K at 15 GPa. Using the strong-coupling-corrected McMillan equation[37,38] with a Coulomb pseudopotential of μ^* = 0.1, we calculated a theoretical T_c of 35.1 K at 15 GPa (Table S1). This value is in agreement with our experimental observation of $T_c \approx 31$ K at 15.6 GPa. This close correspondence between theory and experiment strongly implies that conventional phonon-mediated pairing is the fundamental mechanism underlying the enhanced superconductivity in the SC2 Na-GIC.

Band structure calculations further reveal that the electronic states near the Fermi level are primarily derived from the out-of-plane p_y orbitals of carbon (perpendicular to the graphene layers, given the stacking direction along the b-axis; Figure 4c), with minor contributions from sodium p states. Integration of the Eliashberg phonon spectral function, $\alpha^2F(\omega)$, indicates that approximately 92.0% of the total EPC strength (λ) arises from low-frequency (below 480 cm^{-1}) mixed Na/C vibrations, while the remaining 8.0% is attributed to mid- and high-frequency carbon vibrations (Figure 4d). These results demonstrate that superconductivity in the densely intercalated *Imma*-NaC_3 phase predominantly originates from the strong coupling between carbon π-electrons and low-frequency Na/C phonon modes. Furthermore, our phonon dispersion calculations reveal that the minority $R\bar{3}m$-Na_4C_3 phase is dynamically stable, showing no imaginary modes across the Brillouin zone (Figure S11). Band structure calculations reveal a semiconducting state with a bandgap of 1.3 eV at 15 GPa; thus, its contribution to the observed macroscopic superconductivity is ignorable.

Placing these intrinsic electronic properties into a broader context, we note that while T_c in Na-GICs generally increases with intercalant density—progressing from the stage-2 *Pmma*-NaC_8 phase (maximum $T_c \approx 22.3$ K) to the stage-1 *Imma*-NaC_3 (maximum $T_c \approx 31$ K)—staging alone does not strictly dictate the superconducting properties. The significant T_c variation observed within stage-2 *Cmcm*-NaC_8 ($T_c \approx 28$ K)[25] highlights that specific structural symmetry and atomic coordination are equally crucial in modulating the Fermi surface topology and electron−phonon coupling strength. Furthermore, while superconductivity in GICs is traditionally accounted for by an occupied interlayer state[12,13]—which our calculations confirm for NaC_3 at 15 GPa (Figure S12)—the empirical rule that T_c scales inversely with the interlayer distance[14,23] is challenged in the current work. Despite NaC_3 and CaC_6 possessing nearly identical interlayer distances (2.13 ± 0.02 Å vs 2.15 ± 0.02 Å),[14,23] the maximum T_c of NaC_3 (~31 K) is more than double that of CaC_6 (15.1 K at 7.5 GPa). Ultimately, this demonstrates that high-T_c states in compressed GICs are not governed solely by interlayer distance but emerge from a synergy of high-density stoichiometry, optimal structural symmetry, and enhanced electron−phonon coupling.

The identification of stage-1 *Imma*-NaC_3 structure provides a robust structural foundation for understanding this high-T_c state; however, the rich physics of densely intercalated Na-GICs presents compelling avenues for future exploration. While the proposed model accurately captures the bulk powder diffraction profiles, advanced single-crystal or local-probe investigations will be invaluable for resolving subtle crystallographic nuances, such as local distortions or partial sodium occupancies. These microstructural details become particularly relevant when considering the rapid suppression of T_c as the pressure departs from the 15.6 GPa optimum. Because the calculated pressure dependence of T_c (Table S1) does not fully replicate the observed sharp T_c−P dome, macroscopic superconductivity in this system is likely not governed solely by intrinsic changes in the electronic and vibrational states of an idealized lattice. Instead, microstructural factors—such as interlayer defects, stacking faults, pressure-induced twisting, and pressure-induced structural instabilities[23]—likely play a pivotal role in degrading the superconducting state. Quantitatively disentangling these complex microscopic effects from intrinsic electronic properties remains a formidable, yet highly promising, frontier for high-pressure experimental techniques.[25]

CONCLUSIONS

In summary, we report the realization of a densely intercalated, stage-1 Na-GIC that exhibits bulk superconductivity and achieves a maximum onset T_c of ~31 K under moderate compression. By correlating room-temperature in situ synchrotron X-ray diffraction with first-principles calculations, we identify the host of this superconducting state as an orthorhombic *Imma*-NaC_3 phase, which emerges through a sequence of pressure-driven staging transitions. By elevating the T_c of a carbon-based intercalate above 30 K, this stage-1 Na-GIC bridges the long-standing gap between GICs and the benchmark MgB_2 (T_c = 39 K), establishing these densely packed architectures as a premier platform for exploring high-T_c superconductors. Looking forward, there is a compelling

https://doi.org/10.1021/jacs.6c10866
J. Am. Chem. Soc. 2026, 148, 34888−34894

prospect of retaining this high-pressure metastable phase to ambient pressure via nonequilibrium approaches, such as a low-temperature pressure-quench protocol.[39] Successfully recovering this phase would unlock further optimization of its superconducting properties through compositional tuning and enhanced structural homogeneity, ultimately paving the way for practical applications of lightweight superconductors.

■ ASSOCIATED CONTENT

Data Availability Statement

The data that support the findings of this study are available from the corresponding author upon reasonable request.

Supporting Information

The Supporting Information is available free of charge at https://pubs.acs.org/doi/10.1021/jacs.6c10866.

Synthesis of Na-GIC samples, low-temperature resistance measurements, high-pressure magnetic susceptibility measurements, structural characterization, additional first-principles calculations, MD simulations, and NEP construction (PDF)

Accession Codes

Deposition Numbers 2557294−2557295 contain the supplementary crystallographic data for this paper. These data can be obtained free of charge via the joint Cambridge Crystallographic Data Centre (CCDC) and Fachinformationszentrum Karlsruhe Access Structures service.

■ AUTHOR INFORMATION

Corresponding Authors

Feng Ke − *Center for High Pressure Science, State Key Laboratory of Metastable Materials Science and Technology, Yanshan University, Qinhuangdao 066004, China;* orcid.org/0000-0002-1906-9636; Email: fengke@ysu.edu.cn

Xiang-Feng Zhou − *Key Laboratory of Weak-Light Nonlinear Photonics, School of Physics, Nankai University, Tianjin 300071, China; Center for High Pressure Science, State Key Laboratory of Metastable Materials Science and Technology and Hebei Key Laboratory of Microstructural Material Physics, School of Science, Yanshan University, Qinhuangdao 066004, China;* orcid.org/0000-0001-8651-9273; Email: xfzhou@ysu.edu.cn

Yongjun Tian − *Center for High Pressure Science, State Key Laboratory of Metastable Materials Science and Technology, Yanshan University, Qinhuangdao 066004, China;* orcid.org/0000-0002-4594-4879; Email: fhcl@ysu.edu.cn

Authors

Yuan-Qing Liu − *Key Laboratory of Weak-Light Nonlinear Photonics, School of Physics, Nankai University, Tianjin 300071, China; Center for High Pressure Science, State Key Laboratory of Metastable Materials Science and Technology, Yanshan University, Qinhuangdao 066004, China*

Ming-Xing Huang − *Center for High Pressure Science, State Key Laboratory of Metastable Materials Science and Technology and Hebei Key Laboratory of Microstructural Material Physics, School of Science, Yanshan University, Qinhuangdao 066004, China*

Chun-Mei Hao − *Center for High Pressure Science, State Key Laboratory of Metastable Materials Science and Technology and Hebei Key Laboratory of Microstructural Material Physics, School of Science, Yanshan University, Qinhuangdao 066004, China*

Jingyu Hou − *Center for High Pressure Science, State Key Laboratory of Metastable Materials Science and Technology, Yanshan University, Qinhuangdao 066004, China;* orcid.org/0009-0004-5779-3176

Guochun Yang − *Hebei Key Laboratory of Microstructural Material Physics, School of Science, Yanshan University, Qinhuangdao 066004, China;* orcid.org/0000-0003-3083-472X

Jiajia Feng − *Center for High Pressure Science and Technology Advanced Research, Beijing 100193, China*

Bin Chen − *Center for High Pressure Science and Technology Advanced Research, Beijing 100193, China*

Yang Ding − *Center for High Pressure Science and Technology Advanced Research, Beijing 100193, China*

Shaobo Yu − *National Laboratory of Solid State Microstructures, School of Physics and Collaborative Innovation Center of Advanced Microstructures, Nanjing University, Nanjing 210093, China*

Jian Sun − *National Laboratory of Solid State Microstructures, School of Physics and Collaborative Innovation Center of Advanced Microstructures, Nanjing University, Nanjing 210093, China;* orcid.org/0000-0001-6172-9100

Lin Wang − *Center for High Pressure Science, State Key Laboratory of Metastable Materials Science and Technology, Yanshan University, Qinhuangdao 066004, China*

Bo Xu − *Center for High Pressure Science, State Key Laboratory of Metastable Materials Science and Technology, Yanshan University, Qinhuangdao 066004, China;* orcid.org/0000-0002-9804-1614

Complete contact information is available at: https://pubs.acs.org/10.1021/jacs.6c10866

Author Contributions

#Y-Q. L., M-X. H., and C-M. H. contributed equally to this work.

Notes

The authors declare no competing financial interest.

■ ACKNOWLEDGMENTS

We thank Liling Sun and Shu Cai for helpful discussions on magnetization measurements. This work was supported by the National Key R&D Program of China (Grant Nos. 2022YFA1402300 and 2023YFA1406200) and National Natural Science Foundation of China (Grant Nos. 52288102, 52090020, 52372157). Part of the work was supported by the Hebei Natural Science Foundation (E2025203149 and E2026203211) and the China Postdoctoral Science Foundation (2025M781016). We thank the Shanghai Synchrotron Radiation Facility of BL17UM (31124.02.SSRF.BL17UM) for the assistance with high-pressure synchrotron XRD measurements.

■ REFERENCES

(1) Bardeen, J.; Cooper, L. N.; Schrieffer, J. R. Theory of Superconductivity. *Phys. Rev.* **1957**, *108*, 1175.

(2) Drozdov, A.; Eremets, M.; Troyan, I.; Ksenofontov, V.; Shylin, S. I. Conventional Superconductivity at 203 kelvin at high Pressures in the Sulfur Hydride System. *Nature* **2015**, *525*, 73−76.

(3) Drozdov, A.; Kong, P.; Minkov, V.; Besedin, S.; Kuzovnikov, M.; Mozaffari, S.; Balicas, L.; Balakirev, F. F.; Graf, D.; Prakapenka, V.; et al. Superconductivity at 250 K in Lanthanum Hydride under High Pressures. *Nature* **2019**, *569*, 528−531.
(4) Somayazulu, M.; Ahart, M.; Mishra, A. K.; Geballe, Z. M.; Baldini, M.; Meng, Y.; Struzhkin, V. V.; Hemley, R. J. Evidence for Superconductivity above 260 K in Lanthanum Superhydride at Megabar Pressures. *Phys. Rev. Lett.* **2019**, *122*, 027001.
(5) Nagamatsu, J.; Nakagawa, N.; Muranaka, T.; Zenitani, Y.; Akimitsu, J. Superconductivity at 39 K in Magnesium Diboride. *Nature* **2001**, *410*, 63−64.
(6) Rosner, H.; Kitaigorodsky, A.; Pickett, W. Prediction of High T_c Superconductivity in Hole-Doped LiBC. *Phys. Rev. Lett.* **2002**, *88*, 127001.
(7) Ashcroft, N. Hydrogen Dominant Metallic Alloys: High Temperature Superconductors? *Phys. Rev. Lett.* **2004**, *92*, 187002.
(8) Pickett, W. E. Design for a Room-Temperature Superconductor. *J. Supercond. Novel Magn.* **2007**, *19*, 291−297.
(9) Pickett, W. E. The next Breakthrough in Phonon-Mediated Superconductivity. *Physica C* **2008**, *468*, 126−135.
(10) Lu, S.; Liu, H.; Naumov, I. I.; Meng, S.; Li, Y.; Tse, J. S.; Yang, B.; Hemley, R. J. Superconductivity in Dense Carbon-Based Materials. *Phys. Rev. B* **2016**, *93*, 104509.
(11) Di Cataldo, S.; Qulaghasi, S.; Bachelet, G. B.; Boeri, L. High-T_c Superconductivity in Doped Boron-Carbon Clathrates. *Phys. Rev. B* **2022**, *105*, 064516.
(12) Csányi, G.; Littlewood, P.; Nevidomskyy, A. H.; Pickard, C. J.; Simons, B. The Role of the Interlayer State in the Electronic Structure of Superconducting Graphite Intercalated Compounds. *Nat. Phys.* **2005**, *1*, 42−45.
(13) Calandra, M.; Mauri, F. Theoretical Explanation of Superconductivity in C_6Ca. *Phys. Rev. Lett.* **2005**, *95*, 237002.
(14) Kim, J. S.; Boeri, L.; O'Brien, J. R.; Razavi, F. S.; Kremer, R. K. Superconductivity in Heavy Alkaline-Earth Intercalated Graphites. *Phys. Rev. Lett.* **2007**, *99*, 027001.
(15) Profeta, G.; Calandra, M.; Mauri, F. Phonon-Mediated Superconductivity in Graphene by Lithium Deposition. *Nat. Phys.* **2012**, *8*, 131−134.
(16) Smith, R. P.; Weller, T. E.; Howard, C. A.; Dean, M. P. M.; Rahnejat, K. C.; Saxena, S. S.; Ellerby, M. Superconductivity in Graphite Intercalation Compounds. *Physica C* **2015**, *514*, 50−58.
(17) Yang, S. L.; Sobota, J. A.; Howard, C. A.; Pickard, C. J.; Hashimoto, M.; Lu, D. H.; Mo, S. K.; Kirchmann, P. S.; Shen, Z. X. Superconducting Graphene Sheets in CaC_6 Enabled by Phonon-Mediated Interband Interactions. *Nat. Commun.* **2014**, *5*, 3493.
(18) Heguri, S.; Kawade, N.; Fujisawa, T.; Yamaguchi, A.; Sumiyama, A.; Tanigaki, K.; Kobayashi, M. Superconductivity in the Graphite Intercalation Compound BaC_6. *Phys. Rev. Lett.* **2015**, *114*, 247201.
(19) Hannay, N. B.; Geballe, T. H.; Matthias, B. T.; Andres, K.; Schmidt, P.; MacNair, D. Superconductivity in Graphitic Compounds. *Phys. Rev. Lett.* **1965**, *14*, 225−226.
(20) Weller, T. E.; Ellerby, M.; Saxena, S. S.; Smith, R. P.; Skipper, N. T. Superconductivity in the Intercalated Graphite Compounds C_6Yb and C_6Ca. *Nat. Phys.* **2005**, *1*, 39−41.
(21) Emery, N.; Hérold, C.; d'Astuto, M.; Garcia, V.; Bellin, C.; Marêché, J. F.; Lagrange, P.; Loupias, G. Superconductivity of Bulk CaC_6. *Phys. Rev. Lett.* **2005**, *95*, 087003.
(22) Debessai, M.; Hamlin, J. J.; Schilling, J. S.; Rosenmann, D.; Hinks, D. G.; Claus, H. Superconductivity for CaC_6 to 32 GPa Hydrostatic Pressure. *Phys. Rev. B* **2010**, *82*, 132502.
(23) Gauzzi, A.; Takashima, S.; Takeshita, N.; Terakura, C.; Takagi, H.; Emery, N.; Hérold, C.; Lagrange, P.; Loupias, G. Enhancement of Superconductivity and Evidence of Structural Instability in Intercalated Graphite CaC_6 under High Pressure. *Phys. Rev. Lett.* **2007**, *98*, 067002.
(24) Huang, M.-X.; Liu, Y.-Q.; Hao, C.-M.; Shao, X.; An, T.; Yang, G.; Gao, Y.; Wang, S.; Wang, L.; Xu, B.; Ke, F.; Zhou, X.-F.; Tian, Y. Superconductivity at 22.3 K in Compressed Sodium-Intercalated Graphite. *arXiv* **2025**, arXiv:2509.23137.
(25) Ma, G.; Wang, Y.; Wang, Z.; Nakamoto, Y.; Shimizu, K.; Liu, G.; Zhou, M.; Wang, H.; Gao, P.; Ma, Y. Superconductivity at 28 K in Sodium Graphite Intercalation Compound under High Pressure. *Phys. Rev. Lett.* **2025**, *135*, 166003.
(26) Hao, C.-M.; Li, X.; Oganov, A. R.; Hou, J.; Ding, S.; Ge, Y.; Wang, L.; Dong, X.; Wang, H.-T.; Yang, G.; Zhou, X.-F.; Tian, Y. Superconductivity in Compounds of Sodium-Intercalated Graphite. *Phys. Rev. B* **2023**, *108*, 214507.
(27) Mishra, S. B.; Marcial, E. T.; Debata, S.; Kolmogorov, A. N.; Margine, E. R. Stability-Superconductivity Map for Compressed Na-Intercalated Graphite. *Phys. Rev. B* **2024**, *110*, 174508.
(28) Metrot, A.; Guerard, D.; Billaud, D.; Herold, A. New Results about the Sodium-Graphite System. *Synth. Met.* **1980**, *1*, 363−369.
(29) S, K. P.; Singh, D.; Biswas, P. K.; Hillier, A. D.; Singh, R. P. Superconducting Properties of the Noncentrosymmetric Superconductor LaPtGe. *Phys. Rev. B* **2018**, *98*, 214505.
(30) Buzea, C.; Yamashita, T. Review of the superconducting properties of MgB_2. *Supercond. Sci. Technol.* **2001**, *14*, R115−R146.
(31) Zhu, Y.; Peng, D.; Zhang, E.; Pan, B.; Chen, X.; Chen, L.; Ren, H.; Liu, F.; Hao, Y.; Li, N.; Xing, Z.; Lan, F.; Han, J.; Wang, J.; Jia, D.; Wo, H.; Gu, Y.; Gu, Y.; Ji, L.; Wang, W.; Gou, H.; Shen, Y.; Ying, T.; Chen, X.; Yang, W.; Cao, H.; Zheng, C.; Zeng, Q.; Guo, J.-g.; Zhao, J. Superconductivity in Pressurized Trilayer $La_4Ni_3O_{10-\delta}$ Single Crystals. *Nature* **2024**, *631*, 531−536.
(32) Li, D.; Lee, K.; Wang, B. Y.; Osada, M.; Crossley, S.; Lee, H. R.; Cui, Y.; Hikita, Y.; Hwang, H. Y. Superconductivity in an Infinite-Layer Nickelate. *Nature* **2019**, *572*, 624−627.
(33) Medvedev, S.; McQueen, T. M.; Troyan, I. A.; Palasyuk, T.; Eremets, M. I.; Cava, R. J.; Naghavi, S.; Casper, F.; Ksenofontov, V.; Wortmann, G.; Felser, C. Electronic and Magnetic Phase Diagram of β-$Fe_{1.01}Se$ with Superconductivity at 36.7 K under Pressure. *Nat. Mater.* **2009**, *8*, 630−633.
(34) Miyoshi, K.; Takaichi, Y.; Mutou, E.; Fujiwara, K.; Takeuchi, J. Magnetic Measurements of FeSe Superconductor under High Pressure. *J. Phys. Conf. Ser.* **2010**, *200*, 012126.
(35) Goncharov, A. F.; Zaug, J. M.; Crowhurst, J. C.; Gregoryanz, E. Optical calibration of pressure sensors for high pressures and temperatures. *J. Appl. Phys.* **2005**, *97*, 094917.
(36) Fujii, T.; Ohfuji, H. Pressure estimation using the diamond Raman scale at low pressures in diamond anvil cell experiments using a highly confocal Raman system. *Meas. Sci. Technol.* **2015**, *26*, 025501.
(37) Allen, P. B.; Dynes, R. C. Transition Temperature of Strong-Coupled Superconductors Reanalyzed. *Phys. Rev. B:* **1975**, *12*, 905−922.
(38) Allen, P. B. Theory of Thermal Relaxation of Electrons in Metals. *Phys. Rev. Lett.* **1987**, *59*, 1460−1463.
(39) Deng, L.; Habamahoro, T.; Safezoddeh, A.; Karki, B.; Kazibwe, S.; Schulze, D. J.; Wu, Z.; Julian, M.; Prasankumar, R. P.; Zhou, H.; Smith, J. S.; Hosur, P. R.; Chu, C.-W. Ambient-Pressure 151-K Superconductivity in $HgBa_2Ca_2Cu_3O_{8+\delta}$ via Pressure Quench. *Proc. Natl. Acad. Sci. U. S. A.* **2026**, *123*, No. e2536178123.

https://doi.org/10.1021/jacs.6c10866
J. Am. Chem. Soc. 2026, 148, 34888−34894